

FIRST SOLAR CELL RESULTS ON NOVEL DIRECT-CAST SILICON WAFERS

Philipp Keller¹, Donald Wood², Chris Parfeniuk², Guy Beaucarne², Glen Cook³, Prantik Mazumder³, Giso Hahn¹

¹ University of Konstanz, Department of Physics, Universitätsstr. 10, 78464 Konstanz, Germany

² Dow Corning Europe SA, Parc industriel Rue Jules Bordet, 7180 Seneffe, Belgium

³ Corning Incorporated, One Riverfront Plaza, Corning, NY 14831, USA

Author for correspondence: Philipp.Keller@uni-konstanz.de, Tel.: +49 7531 88 2074, Fax: +49 7531 88 3895

ABSTRACT: Today's costs of silicon wafer material of a photovoltaic module are around 30-40% of its total production costs including feedstock, ingot casting and wafering. Therefore, there is a substantial interest in the development of a kerf-loss free and thus cost-saving silicon wafer production. One method amongst various technologies for direct wafer production is the Direct-Cast Silicon (DCS) process. In this wafer casting process, molten silicon is directly crystallized on a re-usable substrate. The exploration of the solar cell efficiency potential and the characterization of DCS wafer material are of immanent relevance for future development of the DCS technology. A high efficiency solar cell process, developed for defect-rich multicrystalline silicon material at the University of Konstanz, was applied on DCS wafers. IV measurements, Light Beam Induced Current (LBIC) and electroluminescence (EL) were performed. The goal was to gain insight into the material quality and material properties, and to provide feedback for wafer production. Thereby, with 16.0%, the highest solar cell efficiency for this material could be obtained so far.

Keywords: cost reduction, multicrystalline silicon, defects, ribbon silicon, ribbons, kerf loss

1 INTRODUCTION

For reducing material costs in silicon solar cell production, wafer costs are one of the relevant parameters [1, 2]. Around 30-40% of the module costs are caused by the silicon wafers. However, large material losses occur due to slicing wafers from ingots. A solution to these problems can be addressed by a novel direct-cast silicon (DCS) technology [3], which is compatible with the standard industrial PV supply chain. Wafers can be gained without kerf loss at a high wafer production speed in the order of 24 wafers per minute (around 350 cm/min). The wafers are produced by an exocasting process – the controlled crystallization of silicon directly onto the surface of a re-useable substrate, which was high purity fused silica in our case. Control of the exocasting parameters enables control of the critical wafer parameters, including thickness, roughness, grain size, dislocation density and sample doping level. The DCS technique combines the advantages of two ribbon casting techniques. Whereas vertical growth of silicon ribbons, like e.g. in the EFG (Edge-defined Film-fed Growth) [4] process, features a high crystal quality but a low crystallization speed in the order of 1 cm/min, the horizontal growth, like e.g. in the RGS (Ribbon Growth on Substrate) [4] process, gives a high production speed in the order of several 100 cm/min, but poorer crystal quality. The DCS technique operates in a relatively fast crystallization regime (around 350 cm/min) with a good performing crystal quality.

The determination of the solar cell efficiency potential and characterization of DCS material are of immanent relevance for future developments. DCS wafers with a dimension of 5x5 cm² were produced. The wafers feature different areas with small grain sizes and larger grain sizes in the order of some mm² due to the unique crystallization method. In this study we apply a PERC (Passivated Emitter and Rear Cell) solar cell process developed for defect-rich multicrystalline (mc) materials, such as e.g. RST (Ribbon on Sacrificial

Template) [5], RGS, String Ribbon and EFG [6], at the University of Konstanz [7], on DCS wafers and standard mc silicon wafers. The cell process serves as tool for further characterization like IV, LBIC and EL measurements. The goal was to gain insight into the material quality and material properties. A comparison of the cell results allows for determination of limitations and loss mechanisms.

2 MATERIAL AND CELL PROCESS

2.1 DCS material quality

Fig. 1 shows a lifetime calibrated photoluminescence (PL) image of a 5x5 cm² DCS wafer after gettering and hydrogenation by SiN_x:H firing. Areas of different minority carrier lifetimes can clearly be distinguished by the color coding of the PL image. The grain size distribution can be influenced by the wafer casting parameters and is in the order of several mm².

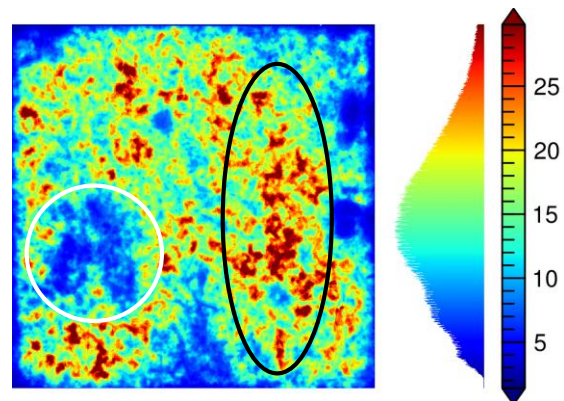


Figure 1: PL image of a 5x5 cm² DCS wafer after gettering and hydrogenation by SiN_x:H firing. Lifetime is calibrated by a QSSPC measurement. The lifetime is heterogeneously distributed. Some areas show reduced lifetime values.

At a minority charge carrier density of $1 \cdot 10^{15} \text{ cm}^{-3}$, the QSSPC measurement of the shown wafer revealed a mean lifetime of about 20 μs . The PL image was done at a minority carrier density of $1.3 \cdot 10^{14} \text{ cm}^{-3}$ resulting in a mean lifetime of 17.0 μs . While small grains (white circle, left in Fig. 1) exhibit poor lifetimes ($\sim 8 \mu\text{s}$), the larger grains (black ellipse, right in Fig. 1) have adequate lifetimes ($\sim 20 \mu\text{s}$) needed for reasonable cell performances. The initial thickness of the DCS wafers in this study is about 230 μm .

2.2 PERC cell process

Besides the DCS wafers some mc references are processed for monitoring the solar cell process. In the photolithography-based PERC cell process four $2 \times 2 \text{ cm}^2$ lab-type solar cells can be obtained from one $5 \times 5 \text{ cm}^2$ wafer. The process flow is depicted in Fig. 2. An anti-reflection coating and passivation of the front side is realized with a silicon nitride layer ($\text{SiN}_x\text{:H}$) done by plasma-enhanced chemical vapor deposition (PECVD). On the rear side (RS) an aluminum oxide (Al_2O_3) layer with a SiN_x capping layer serves as passivation. The back contact is realized with laser fired contacts (LFC) since material and/or cell process induced point shunts were observed on other silicon ribbon materials, e.g. by the commonly applied full Al-BSF process [5]. The contact sintering of the front contacts and an enhanced hydrogen passivation is done by a microwave induced remote hydrogen plasma (MIRHP) step. A double layer anti-reflection coating (DARC) using MgF_2 is applied to the best cells only. More details about the cell process and efficiencies reached on several other silicon materials can be found in [5, 6].

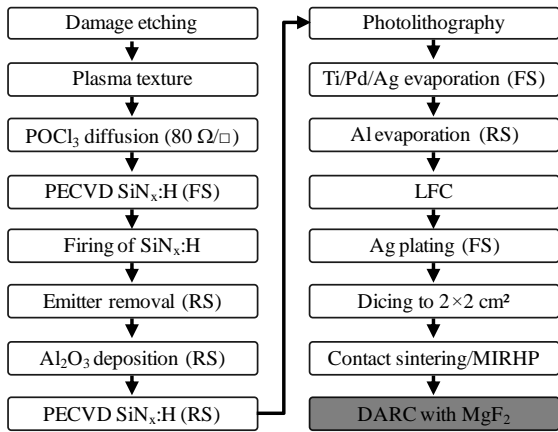


Figure 2: Processing sequence for the photolithography-based PERC cell process with LFCs. DARC is applied to the best cells only.

3 CELL RESULTS

3.1 I-V results

Tab. 1 summarizes the IV-parameters of the cells from this study. The IV measurements are carried out under AM 1.5G illumination at 25°C. The average value and the standard deviation of 13 DCS cells and 6 mc cells are shown. The best cell results obtained with a single layer anti-reflection coating (SARC) on plasma textured surface is also shown in Tab. 1 denoted with “SARC”.

Table 1: Averaged IV-parameters of all solar cells from DCS and the references with SARC. DCS: 13 cells, mc: 6 cells. The best cells from DCS (with SARC and DARC) and mc are also shown.

Group (quantity)	V_{oc} (mV)	J_{sc} (mA/cm^2)	FF (%)	η (%)
DCS (13)	593 ± 4	34.2 ± 0.4	73.5 ± 3.3	14.9 ± 0.9
DCS _{SARC}	600	34.9	76.0	15.9
DCS _{DARC}	595	35.5	76.0	16.0
mc (6)	623 ± 3	36.1 ± 0.1	75.4 ± 2.5	17.0 ± 0.7
mc _{best}	625	36.1	78.2	17.6

With SARC a highest efficiency of 15.9% on DCS wafers is demonstrated. Applying a DARC with MgF_2 on the best DCS cell leads to an increase of only 0.1%_{abs} in efficiency. Thus, 16.0% is the highest efficiency obtained so far on this kind of wafer material. j_{sc} could be improved by 0.6 mA/cm^2 to 35.5 mA/cm^2 . However, the open circuit voltage V_{oc} unexpectedly suffered from the DARC process by 5 mV. As the cell process was not totally stable at the time of processing, we therefore think that using a more stable cell process allows for even higher values. j_{sc} is with a mean of 34.2 mA/cm^2 at a good level, but probably suffers from the smaller grains. Compared to standard multicrystalline silicon cells with a mean value of 36.1 mA/cm^2 with SARC, there is still room for further improvement. V_{oc} is limited to 600 mV which already demonstrates a good crystal quality. Although this is already a reasonable value for direct-cast wafer cells, further measurements, like SR LBIC and EL, are carried out to determine the limiting factors for V_{oc} . The fill factor is with up to 76.0% close to the mc reference cells which have an average of 75.4% but exceed 78.0% in the maximum. In total, the mean efficiencies with SARC of the DCS cells are 14.9% and 17.0% for the mc cells, respectively. Thus, the gap to the mc reference is 2.1%. Even better cell results are expected on further improved DCS wafers and a more stable cell process. With these first measurements the cell process can be modified to further push the efficiencies of DCS wafer cells to higher values.

3.2 SR measurements

In Fig. 3 the Internal Quantum Efficiencies (IQEs) measured via spectral response of one of the best DCS cells (red circles) and a block-cast mc reference cell (black squares) are shown. The IQE gives depth dependent information about the solar cell. The emitter on both cells, mc reference and DCS, behaves similar up to a wavelength of 600 nm. Beginning from 700 nm, which corresponds to a penetration depth of $>5 \mu\text{m}$, the IQE of the DCS cell constantly drops beneath the IQE of the mc cell. These limitations indicate variations in material quality and can be contributed to the smaller grain sizes and limited material quality of DCS. A local minimum of the first derivative of the IQE from the DCS cell gives an indication of a kink in the IQE at 980 nm ($d_p=100 \mu\text{m}$). This points to the fact that the PERC cell structure has a positive influence and enhances the long wavelength quantum response. Charge carriers which are generated at a depth of 100-200 μm can contribute to the current.

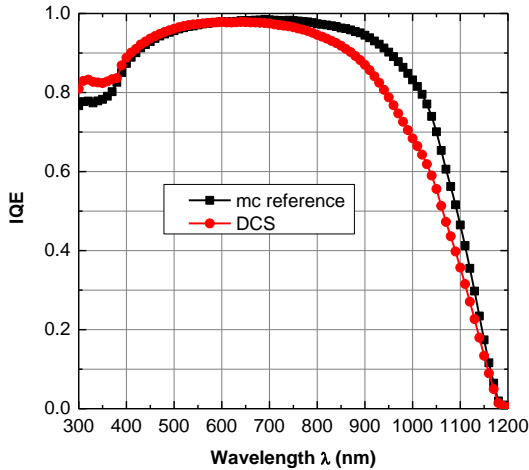


Figure 3: IQE of the best DCS cell (red circles) and a block-cast mc reference cell (black squares).

The effective minority charge carrier diffusion length L_{eff} is extracted by a fit to the long wavelength IQE curves using an IQE evaluation program from Fischer [8].

Hereby, mean values in the range of 150-220 μm for DCS cells and $\sim 580 \mu\text{m}$ for the mc reference cell are obtained. L_{eff} of the DCS cells is in the order of the cell thickness; hence, a good rear surface passivation is crucial which is realized with a SiN_x capped Al_2O_3 layer in our case.

3.3 LBIC investigations

LBIC measurements are carried out on DCS cells to spatially determine material quality. The laser excitation wavelengths are 833 nm, 910 nm and 980 nm corresponding to penetration depths d_p of 15 μm , 36 μm and 103 μm , respectively. The IQE maps with a resolution of 20 $\mu\text{m}/\text{px}$ of a DCS cell are shown in Fig. 4. The red square marks an area with a high density of strong recombination active grain boundaries (GB) whereas the directly neighboring black square frames an area with nearly no recombination active GBs. It is obvious that the recombination active GBs lead to a loss in the long wavelength IQE signal compared to areas with no recombination active GBs or larger grains, respectively. At a penetration depth of about 15 μm (833 nm) the examined recombination active cluster exhibits IQE values of about 0.82. This value drops in the direction of the rear side of the solar cell dramatically to 0.69 at a penetration depth of 36 μm (910 nm) and 0.49 at a penetration depth of 103 μm (980 nm). This is a loss of nearly 40% in the quantum efficiency. This fact can also be seen on the distributions of the IQE values which broaden to longer wavelength. On the other hand, the comparably low/not recombination active site (black squared region) shows good IQE values for all investigated wavelengths. Starting at 0.9 at 15 μm (833 nm), the value drops to 0.82 at 36 μm (910 nm) and 0.69 at 103 μm (980 nm). This is a loss of just 24%. There are even areas which exceed an IQE value of 0.8 (980 nm) at some points (indicated by an arrow in Fig. 4). The highly recombination active GB clusters are one reason for the lower performing IQE of DCS cells in the long wavelength region. With the spatial measurement of the IQE at different wavelengths it is possible to calculate L_{eff} with a model according to Basore [9]. The result of the calculation can be seen in Fig. 5.

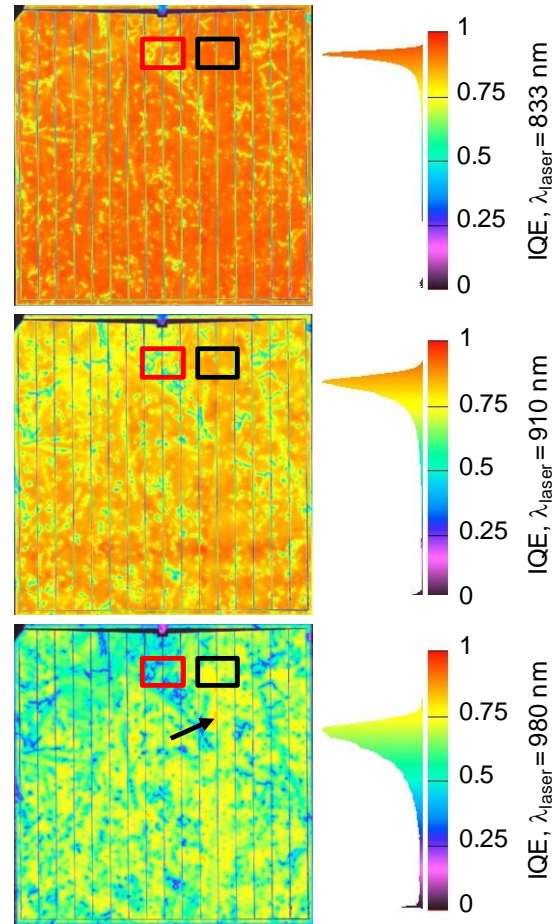


Figure 4: LBIC maps of a 2x2 cm² DCS cell with different laser wavelengths: 830 nm (top), 910 nm (middle) and 980 nm (bottom). Exemplarily strongly recombination active areas (left, red) and good performing areas (right, black) are marked by squares.

The investigated cell exhibits a mean value of $L_{\text{eff}}=142 \mu\text{m}$ and a peak value of $L_{\text{eff,peak}}=171 \mu\text{m}$. The L_{eff} values are quasi-Gaussian distributed which is beneficial for cell performance. In contrast, e.g. EFG cells can exhibit areas with quite low performing IQEs altering with areas of very high IQE values [6]. This leads to a distribution of L_{eff} with more than one peak which is a limiting factor to the cells performance.

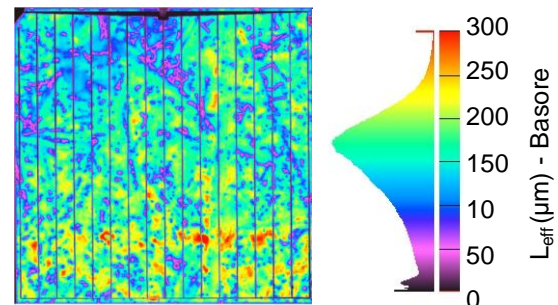


Figure 5: L_{eff} map of a 2x2 cm² DCS cell calculated using a model according to Basore [9]. The values are quasi Gaussian distributed with a mean value of $L_{\text{eff}}=142 \mu\text{m}$.

3.4 Electroluminescence measurements

For further analysis the DCS cells were measured by EL under different excitation currents ranging from 5 mA/cm^2 to 50 mA/cm^2 . A mid performing cell with $j_{sc}=33.5 \text{ mA/cm}^2$ and $V_{oc}=586 \text{ mV}$ is shown in Fig. 6. The excitation current in this case is 5 mA/cm^2 and the measurement time is 120 s. Charge carriers are injected into the cell by an external power source. Band-to-band recombination in good crystal regions leads to a strong EL signal whereas recombination via defect states as e.g. in grain boundaries does not lead to band-to-band luminescence. Thus, high densities of defects and grain boundaries lead to low EL intensities as can be seen in Fig. 6. Comparing the result of the EL measurement with the LBIC measurement of Fig. 4 a good correlation is clearly obvious. GBs and areas which exhibit minor L_{eff} values show also a low EL signal and thus a reducing influence on the voltage. Both, V_{oc} and j_{sc} suffer from recombination active defects and GBs, leading to a limitation of cell performance compared to mono crystalline silicon cells.

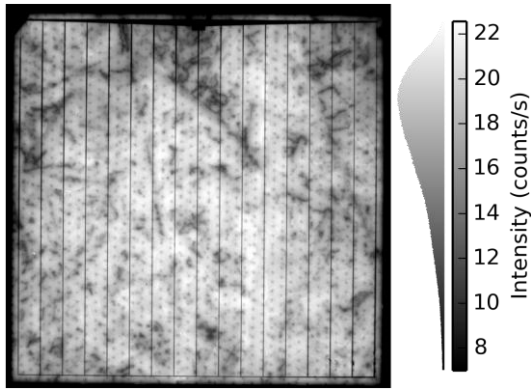


Figure 6: EL map of a DCS cell. The excitation current is 5 mA/cm^2 and measurement time is 120 s.

The series resistance (R_s) and the dark saturation current (j_0) can be calculated by a model suggested by Breitenstein et al. [10]. For this purpose EL images with different excitation currents are computed. Hence, the cell of Fig. 6 was measured at 5 mA/cm^2 and 40 mA/cm^2 resulting in the maps shown in Fig. 7.

The cell is contacted on the busbar located at the top of Fig. 7. Therefore, R_s is asymmetrically distributed and rises towards the bottom side of the cell. The average of R_s is in the range of $0.25 \Omega\text{cm}^2$ which is at a really good level. But, on the other hand, an R_s issue in the upper right corner of the cell is noticeable. The question of the origin of the contact problem can be answered by a comparison with the dark saturation current image. The area of the contact issue coincides with an area of relatively but not extraordinarily high j_0 values (similar values can be seen in other cell areas as well, not causing R_s problems). If the contact problem would be material induced, high R_s values should also appear at other positions on the cell which exhibit poor j_0 values. Since this is not the case the contact problem might probably solar cell process induced (e.g. due to the cell process not being totally stable at the time of processing). In total, contact issues show consequences for the fill factor which is hence reduced. Regions which appear dark in the EL map give a high j_0 value.

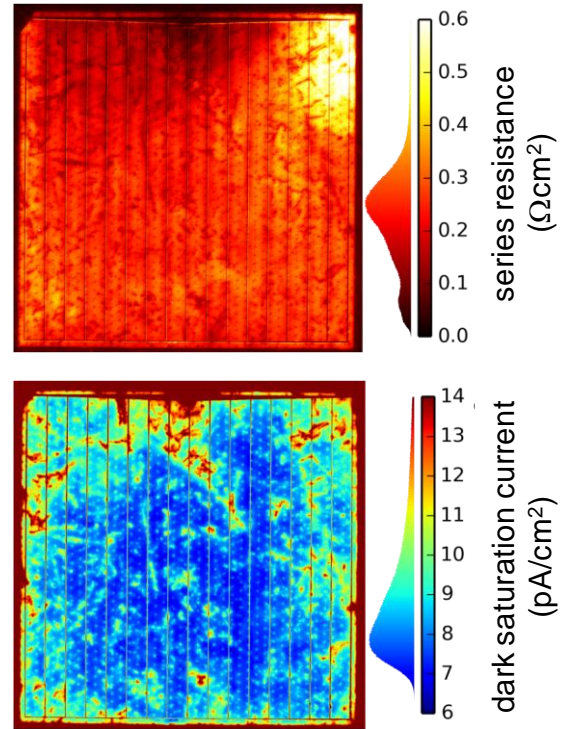


Figure 7: Spatially resolved series resistance (top) and dark saturation current density (bottom) of a DCS cell (see Fig. 6). The values are extracted using a model of Breitenstein et al. [10].

Not all grain boundaries appear in the EL image and from those which are visible, different intensities in the j_0 image can be measured. This leads to the assumption that the GBs and defect sites exhibit a different degree of impurity decoration and/or may respond differently to gettering steps. The cell shown in Fig. 7 exhibits a j_0 of 9.3 pA/cm^2 .

4 CONCLUSION

Solar cell results on a novel type of Si ribbon are presented. The new direct-cast silicon method allows for ultra-low cost, fast and kerf-loss free silicon wafer technology. In this new wafer casting process, molten silicon is directly crystallized on a re-useable substrate. A high wafer production speed in the order of 10 wafers per minute is possible. A photolithography-based lab-type PERC solar cell process was applied on the ribbon silicon wafers. Thus, the material potential could be estimated and both the material quality and the specific material properties could be investigated. DCS and standard mc wafers were processed and compared. LBIC, EL and SR measurements showed the limitation of the material specific defects. A maximum efficiency with a SARC of 15.9% and with a DARC of 16.0% was obtained on a $2 \times 2 \text{ cm}^2$ DCS cell which is the highest value published so far for this material.

5 ACKNOWLEDGEMENTS

Dow Corning for funding and the team at Dow Corning and Corning Inc. for providing the wafer material and the good cooperation. Part of this work was financially

supported by the German Federal Ministry for the Environment, Nature Conservation and Nuclear Safety (FKZ 0325581). The content is the responsibility of the authors.

6 REFERENCES

- [1] D.M. Powell, M.T. Winkler, H.J. Choi, C.B. Simmons, D. Berney Needleman, T. Buonassisi, Crystalline silicon photovoltaics: a cost analysis framework for determining technology pathways to reach baseload electricity costs, *Energy Environ Sci* 5, 2012, pp. 5874-83.
- [2] A. Goodrich et al., A wafer-based monocrystalline silicon photovoltaics road map: Utilizing known technology improvement opportunities for further reductions in manufacturing costs, *Sol. Energy Mater. Sol. Cells* 114, 110-135, 2013, pp. 111-35.
- [3] G.B. Cook, P. Mazumder, K.K. Soni, B. Suman, C.S. Thomas, N. Venkataraman, Methods of making an unsupported article of pure or doped semiconducting material, US Pat. No. 8617447.
- [4] G. Hahn, S. Seren, M. Kaes, A. Schonecker, J.P. Kalejs, C. Dube, A. Grenko, C. Belouet, Review on ribbon silicon techniques for cost reduction in PV, *Proc. 4th WCPEC, Waikoloa, 2006*, pp. 972-5.
- [5] P. Keller, U. Hess, S. Seren, J. Junge, F. de Moro, G. Hahn, Over 14% efficiency on RST-ribbon solar cells, *Proc. 27th EU PVSEC, Frankfurt, 2012*, pp. 2053-7.
- [6] J. Junge, J. Ebser, S. Graf, B. Terheiden, S. Seren, G. Hahn, M. Käs, Evaluating the efficiency limits of low cost mc Si materials using advanced solar cell processes, *Proc. 25th EU PVSEC, Valencia, 2010*, pp. 1722-6.
- [7] J. Junge, C. Srümpel, S. Seren, G. Hahn, A. Metz, M. Käs, Laser Fired Contacts for high efficiency solar cells based on EFG material, *Proc. 23rd EU PVSEC, Valencia, 2008*, pp. 1561-3.
- [8] B. Fischer, Loss analysis of crystalline silicon solar cells using photoconductance and quantum efficiency measurements, Ph.D. thesis, University Konstanz, 2003.
- [9] P. A. Basore, Extended spectral analysis of internal quantum efficiency, in *Proceedings 23rd IEEE PVSC, 1993*, pp. 147-52.
- [10] O. Breitenstein, A. Khanna, Y. Augarten, J. Bauer, J.-M. Wagner, K. Iwig, Quantitative evaluation of electroluminescence images of solar cells, *Physica Status Solidi RRL* 4 (1), 2010, pp. 7-9.